



1 Evaluation of a reduced pressure chemical ion reactor utilizing
2 adduct ionization for the detection of gaseous organic and
3 inorganic species

4

5 Matthieu Riva^{1,2, †,*}, Veronika Pospisilova^{1, †}, Carla Frege¹, Sebastien Perrier², Priyanka Bansal¹,
6 Spiro Jorga¹, Patrick Sturm¹, Joel A. Thornton³, Urs Rohner¹, Felipe Lopez-Hilfiker^{1,*}

7 ¹ TOFWERK, 3645 Thun, Switzerland

8 ² Université Claude Bernard Lyon 1 CNRS, IRCELYON 69626, Villeurbanne France

9 ³ Department of Atmospheric Sciences, University of Washington, Seattle, Washington 98195,
10 USA.

11

12 *Correspondence to:* matthieu.riva@tofwerk.com & lopez@tofwerk.com

13 [†] These authors contributed equally.

14

15

16

17



18 **Abstract**

19 Volatile organic compounds (VOCs) and volatile inorganic compounds (VICs) provide critical information
20 across many scientific fields including atmospheric chemistry, soil, and biological processes. Chemical
21 ionization (CI) mass spectrometry has become a powerful tool for tracking these chemically complex and
22 temporally variable compounds in a variety of laboratory and field environments. It is particularly powerful
23 with time-of-flight mass spectrometers, which can measure hundreds of compounds in a fraction of a second
24 and have enabled entirely new branches of VOC/VIC research in atmospheric and biological chemistry. To
25 accurately describe each step of these chemical, physical, and biological processes, measurements across
26 the entire range of gaseous products is crucial. Recently, chemically comprehensive gas-phase
27 measurements have been performed using many CI mass spectrometers deployed in parallel, each utilizing
28 a different ionization method to cover a broad range of compounds. Here we introduce the recently
29 developed Vocus AIM (Adduct Ionization Mechanism) ion-molecule reactor (IMR), which samples trace
30 vapors in air and ionizes them via chemical ionization at medium pressures. The Vocus AIM supports the
31 use of many different reagent ions of positive and negative polarity and is largely independent of changes
32 in the sample humidity. Within the present study, we present the performance and explore the capabilities
33 of the Vocus AIM using various chemical ionization schemes, including Chloride (Cl^-), Bromide (Br^-),
34 Iodide (I^-), Nitrate (NO_3^-), Benzene cations (C_6H_6^+), Acetone dimers ($(\text{C}_3\text{H}_6\text{O})_2\text{H}^+$), and Ammonium
35 (NH_4^+) reagent ions primarily in laboratory and flow tube experiments. We report the technical
36 characteristics, operational principles, and compare its performance in terms of time response, humidity
37 dependence, and sensitivity to that of previous chemical ionization approaches. This work demonstrates the
38 benefits of the Vocus AIM reactor which provides a versatile platform to characterize VOCs and VICs in
39 real time at trace concentrations.

40



41 1. Introduction

42 Mass spectrometry represents a nearly universal method for determining the chemical composition of
43 organic and inorganic species across various environmental matrices. In the fields of environmental and
44 atmospheric chemistry, chemical ionization (CI) is a versatile real-time method to measure individual
45 organic and inorganic compounds in air at trace concentrations (Yuan et al., 2017; Riva et al., 2019; Zhang
46 W. et al., 2023; Zhang Y. et al., 2023). As in all chemical ionization systems, trace analytes in air react with
47 excess reagent ions, leading to the formation of charged product ions usually via electron/proton transfer
48 or adduct formation (Zhang W. et al., 2023; Zhang Y. et al., 2023). Advances in the field of chemical
49 ionization over the last decade have yielded exceptionally low detection limits down to 10^4 molecules cm^{-3}
50 (part-per-quadrillion), expanded dynamic ranges, and the capability of measuring a wide range of gaseous
51 organic and inorganic species with time resolutions of up to 50 Hz (Riva et al., 2019; Zhang W. et al., 2023;
52 Zhang Y. et al., 2023).

53 Chemical ionization mass spectrometers are uniquely able to measure temporal variability of trace
54 VOC and atmospheric oxidation products; both in the laboratory and in the field, providing a critical tool
55 to mechanistically track the most important atmospheric oxidation processes (Hallquist et al., 2009, Ehn et
56 al., 2014, Bianchi et al., 2019). In particular, CI has made enormous improvements in the detection and
57 quantification of reactive gaseous oxygenated species, including peroxy (RO_2) radicals, stabilized Criegee
58 intermediates, and inorganic acids and bases which are difficult to directly detect with any other available
59 analytical technique (Berndt et al., 2015, 2017, 2018; Breitenlechner et al., 2017; Hansel et al., 2018;
60 Krechmer et al., 2018). For example, measurements via chemical ionization mass spectrometry (CIMS)
61 have been pivotal in discovering the existence and importance of extremely low volatility organic molecules
62 (ELVOCs). These compounds are now understood to be formed ubiquitously in the atmosphere and are
63 critical to new particle formation and growth (Ehn et al., 2014; Bianchi et al., 2019). As a result, CIMS has
64 emerged as a core analytical tool in atmospheric chemistry and related fields which require high sensitivity,
65 high temporal resolution, and molecular-level speciation (Bruderer et al., 2019; Riva et al., 2019; Tang et
66 al., 2019; Mazzucotelli et al., 2022; Zhang W. et al., 2023; Zhang Y. et al., 2023).



67 With the right selection of reagent ions, CI offers the possibility of soft, selective, and sensitive
68 online detection, for essentially any class of chemical compounds. While in practice, no reagent ion can
69 simultaneously detect the entire distribution of volatile compounds present in the atmosphere with sufficient
70 selectivity and sensitivity, different reagent ions can be selected to target distinct chemical families
71 (Crouse et al., 2006; Bertram et al., 2011, 2016; Lee et al., 2014, Bianchi et al., 2019, Riva et al., 2019;
72 Zhang W. et al., 2023; Zhang Y. et al., 2023). Therefore, a critical choice for chemical ionization operators
73 is which reagent ion is best suited to measure compounds of interest in each measurement scenario.

74 Recent advancements in the design of the reactor have sought to improve measurement quality by
75 addressing two outstanding limitations of chemical ionization mass spectrometers: (i) improved detection
76 efficiency by refining the reactor geometry and optimizing the flow dynamics within the system, and (ii)
77 reliable, reproducible, and fully controlled reaction conditions. Improvements in the detection efficiency
78 depend on the balance of two critical parameters in any chemical ionization reactor. First, compounds
79 present in the sample gas stream need to be efficiently transported to the reaction cell and mix/react with
80 the reagent ions. The efficiency of the first step depends primarily on ionization pressure and absolute flow
81 rate (i.e., residence time). At atmospheric pressure, gases diffuse slowly, and maintaining laminar flows
82 between the sample line and reaction cell is straightforward (e.g., Eisele-inlet, MION, Crossflow CIMS)
83 (Eisele and Tanner, 1993; Palm et al., 2019; Rissanen et al., 2019, Pfeifer et al., 2020). However, operating
84 at high pressure makes controlling ionization conditions much more challenging. Therefore, most CIMS
85 instruments operated at a reduced pressure to facilitate control of the ionization conditions. Sample vapors
86 enter most reduced-pressure chemical ionization mass spectrometers through a critical orifice, which
87 introduces turbulence as the gas expands into the reaction cell. These turbulences can introduce contact
88 between the neutral sample gas and the reactor walls, resulting in memory effects and losses of reactive
89 trace compounds by collision with the walls. While there have been numerous efforts to improve the
90 introduction of sample gases into reduced pressure reactors by laminarizing (Palm et al., 2019) the incoming
91 airflow or controlling the expansion inside of specially coated glass tubes (Vasquez et al., 2018), these
92 approaches are often complex and demand considerable optimization, which has hindered their widespread



93 adoption. Consequently, turbulent wall losses and memory effects continue to pose substantial challenges
94 in reduced-pressure chemical ionization instruments, particularly when detecting reactive or sticky
95 compounds.

96 Operating chemical ionization instruments at reduced pressure provides more refined control over
97 ion chemistry since it allows for more straightforward and effective manipulation of ions within the
98 instrument. Of particular nuisance in nearly all chemical ionization approaches is water vapor, which is
99 highly variable and can have significant effects on the chemical ionization process. The formation of water
100 clusters, which grow rapidly as a function of increasing pressure, presents a specific challenge for
101 measurements taken near atmospheric pressure. Even chemical ionization approaches that operate at low
102 pressures like proton transfer reaction (PTR) can be affected by the presence of water vapor (Yuan et al.,
103 2017). PTR instruments are widely used for the detection of trace VOC using high electric fields to control
104 the reagent ion populations under changing humidity. While PTR instruments can largely control the
105 ionization and collision conditions in the reactor, applying high electric fields results in extensive
106 fragmentation of some critical functional groups in many fields (Yuan et al., 2017). Further, the PTR
107 ionization process is well known to lead to significant fragmentation of labile compounds such as acids,
108 peroxides, and alcohols. The fragmentation induced by protonation or charge transfer reactions along with
109 elevated collision energy within the reactor significantly complicates the mass spectrum, in some cases
110 limiting the possibility of retrieving the accurate concentration and composition of many classes of
111 compounds including highly oxygenated and functionalized organic species.

112 To improve the sensitivity (specificity) and reduce the degree of fragmentation, softer chemical
113 ionization techniques relying on adduct formation have become increasingly popular, especially when
114 molecular identification and mechanistic pathways must be accurately tracked. These reactors operate under
115 low ($E/N < 10$ Td) or field-free conditions at pressures (typically 50-500 mbar), to promote adduct formation
116 and stabilization (Zhang W. et al., 2023; Zhang Y. et al., 2023). Fluid dynamics and the degree of turbulence
117 inside the reactor govern reaction times and ion transport in such reactors. At these elevated ionization
118 pressures, the effect of water vapor can become a critical parameter affecting sensitivity. Routinely used



119 reagent ions can result in order of magnitude changes in sensitivity under atmospherically relevant
120 fluctuations of humidity (Lee et al., 2014; Breitenlechner et al., 2017; Zhang W. et al., 2023; Zhang Y. et
121 al., 2023). Correcting the data for each compound's humidity dependence is an error-prone and time-
122 consuming process where each compound must be treated essentially individually. Flooding the reactor
123 with water vapor, as done in techniques like Vocus PTR, can suppress the humidity dependence of some
124 compounds. Such approaches are only applicable to certain groups of compounds whose water vapor
125 dependence becomes weaker at higher absolute concentrations of water, which is not a universal
126 characteristic. In general, the lack of adequate water vapor control remains a major drawback of chemical
127 ionization systems most critically those operated at pressures greater than 10 mbar.

128 Herein we introduce the Vocus AIM ion molecule reactor (IMR) and report the technical
129 characteristics, operation principle, and performance of this new chemical reactor. We evaluate its
130 performance by reporting the time response of nitric acid, demonstrating a novel approach to suppress
131 humidity dependence, and comparing sensitivity to other CI reactors. We present the design and capabilities
132 of the Vocus AIM using a wide variety of reagent ions, including Chloride (Cl^-), Bromide (Br^-), Iodide (I^-
133), Nitrate (NO_3^-), Benzene cations (C_6H_6^+), Acetone dimers ($(\text{C}_2\text{H}_5\text{O})_2\text{H}^+$), and Ammonium (NH_4^+) ions.
134 Finally, we show the measurement of RO_2 radicals and oxygenated VOCs acquired during the proof-of-
135 concept experiment of OH/O_3 -initiated oxidation of α -pinene. This work highlights the benefits of the
136 Vocus AIM reactor within atmospheric chemistry and its limitations.

137 2. Experimental Section

138 2.1. Vocus AIM Reactor Design

139 Medium pressure chemical ionization (20-500 mbar) systems are typically designed as flow tube reactors
140 which primarily transport ions toward the reactor exit by gas flow. Manipulating ions at high pressure would
141 require high electric fields which are either impractical or could fragment the labile analyte ions. Further,
142 RF devices that could focus ions into a beam, do not efficiently operate at such high pressures, precluding
143 their efficient use. Therefore, the Vocus AIM reactor operates on many of the same fundamental principles



144 of more traditional flow tube reactors, including field-free ionization conditions (Figure 1) and fluid
145 dynamic transport of ions through the reactor. Specifically, the new design includes improvements in
146 sample and reagent ion introduction, a conductive polytetrafluoroethylene (cPTFE) Teflon conical reaction
147 chamber to improve time response, and a simple yet efficient quadrupole based differentially pumped TOF
148 interface.

149 Gases enter the reactor manifold via a 1/2" O.D. Swagelok fitting which is pumped through an inlet
150 via a radially symmetric pump port. Excess flow is used to maintain short residence time and to minimize
151 inlet memory effects such as surface reaction (conversion) and irreversible wall losses. Typical make-up
152 flow rates of 5-10 standard liters per minute (slpm) are used to transport neutral analytes efficiently to the
153 entrance of the reactor. A bored through Swagelok interface ensures that all wetted surfaces before the
154 reactor are Teflon®, to minimize the retention and memory of the inlet line for semi-volatile gases and
155 reduce surface activity. At the entrance of the Vocus AIM IMR, the sample flow enters directly into the
156 center of the conical reactor at a flow rate of 1.8 slpm through a stainless-steel critical orifice (0.475 mm)
157 and a PFA Teflon® sample flow guide which promotes subsampling from the center of the laminar inlet
158 flow. The reactor is typically operated at a pressure of 50 mbar as a compromise between sensitivity and
159 linear range and is controlled by a pressure control valve and an IDP3 vacuum pump (Agilent Technologies,
160 IDP3). The reactor is temperature controlled to 50 °C, which is the lowest temperature that can be reliably
161 controlled across various field conditions to ensure constant reaction conditions. While a lower reactor
162 temperature would promote adduct formation, the long-term stability of thermal conditions would be more
163 difficult to maintain. Reagent ions are generated by compact Vacuum Ultra-Violet (VUV) ion sources
164 arranged radially around the central axis with reactant ions injected at an angle (45 degrees) to intersect the
165 expanding sample flow with minimal sample deflection and ensure that no VUV light directly enters the
166 IMR. Each ion source introduces the ions into the reactor with a standard flow rate of 0.25 slpm for optimum
167 reagent ion yield (Figure S1), nearly an order of magnitude lower flows than polonium or X-ray based ion
168 sources typically used. The residence time inside the reactor under these standard conditions is ~ 10 ms.



169 Modeled flow velocities in the Vocus AIM IMR (Figure 1) were used to optimize the flow patterns
170 inside the reaction cell. The velocity field shows the intersection of the reagent ion jet with the sample flow
171 and was optimized to minimize the contact of sample gas with reactor surfaces as well as to prevent
172 turbulent eddies near the gas expansion region. The gas flow dynamics were modeled with the open-source
173 computational fluid dynamics (CFD) software OpenFOAM v8 (<https://openfoam.org/>) using a customized
174 solver (<https://github.com/pasturm/rhoReactingPimpleFoam>) to simulate supersonic flow in a vacuum with
175 mixing of different gases. The final geometry is constrained by machinability (finite tool dimensions) while
176 also minimizing the response time and reducing reactive and ion wall losses.

177 2.2 Reagent Ion Generation

178 Compact VUV ion sources generate reagent ions by converting photons from a VUV lamp (UV Lamp
179 Krypton DC PID PKS 106, Hereaus) at two wavelength bands corresponding to energies of ~10.0 and 10.6
180 eV into the desired reagent ions (Ji et al., 2020; Breitenlechner et al., 2022). As in prior work, we utilize a
181 primary photo-absorber (e.g., benzene) as a source of photoelectrons and directly formed cations to generate
182 subsequent reagent ions. Permeation tubes are held at 80 °C in a compact oven and deliver constant amounts
183 of corresponding photo-absorber and reagent ion precursor into the 0.250 slpm UHP nitrogen stream.
184 Gaseous benzene (C₆H₆, Sigma Aldrich, ≥99.9%) delivered from the permeation tube, enters the VUV lamp
185 housing and is photoionized (with an absorption cross-section of 4 x 10¹⁷ cm² molecule⁻¹ and ionization
186 potential = 9.24 eV), yielding C₆H₆⁺ and photoelectrons (Lavi et al., 2018). By mixing benzene with trace
187 methyl iodide (CH₃I, Sigma Aldrich, 99.8%), bromoethane (C₂H₅Br, Sigma Aldrich, ≥99%) or nitric acid
188 (HNO₃, Sigma Aldrich, ≥65.6%), various anions such as I⁻, Br⁻, or NO₃⁻ are generated alongside with C₆H₆⁺
189 following reactions equations (1 and 2) and are introduced into the Vocus AIM reactor. A small aperture at
190 the exit of the illuminated region of the ion source prevents back-diffusion of sample air into the primary
191 ionization chamber.

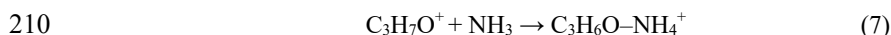
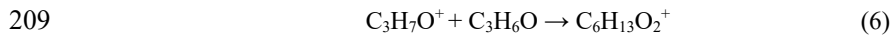
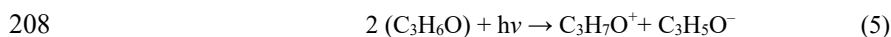




194 By manipulating the above mechanisms, other reagent ions can be readily produced in high abundance and
195 high purity. Cl^- reagent ions can also be produced by introducing 0.250 slpm of UHP nitrogen through the
196 permeation tube oven containing pure dichloromethane (CH_2Cl_2 , Sigma Aldrich, $\geq 99.8\%$) permeation tube.
197 Once formed, anion reagent ions mix with the sample flow in the main reaction chamber and ionize the
198 compounds of interest (M) through the reactions described in equations (3 and 4), with X being I^- , Br^- , Cl^-
199 or $(\text{HNO}_3)_n\text{NO}_3^-$ ($n = 0, 1, 2$).



202 To generate ammonium ions, we irradiate gaseous acetone with VUV light, which results in self-protonated
203 acetone (5) and directly reacts with the acetone molecules yielding protonated acetone dimers (6) (Dong et
204 al., 2022). A continuous flow of NH_3 , typically a few sccm, (i.e., $[\text{NH}_3] > 100$ ppm) from a 1% gas cylinder
205 (in nitrogen) can be introduced directly into the VUV source along with the acetone (Figure 1), NH_3
206 molecules react with the protonated acetone yielding acetone-ammonia adducts which can be used for
207 subsequent ionization in the main reaction chamber (7).



211 Similar to anion reagent ions, these positive ions can ionize the compounds of interest through either adduct
212 formation or proton transfer or in the case of benzene, charge transfer. At pressures of 50 mbar, most
213 chemical ionization reactions occur via ligand switching reactions involving the analyte and hydrated
214 reagent ions.

215 To minimize the effect of water vapor during the ionization process inside the IMR, a water vapor
216 control system consisting of a regulated flow of a dopant (i.e., organic compound) can be injected directly
217 into the IMR (Figure 1). By replacing water with a stable concentration of the dopant, a stable ion
218 distribution is obtained across the entire range of relative humidity (RH) (further discussed in section 3.2).



219 2.4 Vacuum Interface and Analyzer

220 At the exit of the Vocus AIM reactor, product ions are sampled through a 1 mm orifice into the differentially
221 pumped vacuum interface. The efficiency with which the ions at the end of the reactor are sampled depends
222 primarily on the ratio of the sample flow which exits through the orifice relative to the flow towards the
223 vacuum pump evacuating the reaction chamber. This flow split is in turn also dependent on the reactor
224 pressure but is typically ~ 0.5 slpm. After entering the next stage of the interface, an RF-only quadrupole
225 ion guide efficiently focuses the analyte ions into a narrow beam, leading to the net removal of the neutral
226 molecules by a vacuum pump (Ebara PDV 500). Typical RF amplitudes of $100 V_{p-p}$ are sufficient to focus
227 most ions without significant ion activation for the iodide-water adduct where the iodide-water adduct is a
228 very weakly bound complex that is known to respond to transfer through vacuum interfaces relative to its
229 known thermodynamic distribution. In general, reagent ions and analyte ions that are very weakly bound
230 to the reagent ions (e.g., water cluster with a binding energy of 42 kcal/mol) (Caldwell et al., 1989) are
231 often observed to deviate from the thermodynamic distribution with RF amplitudes $>50 V_{p-p}$. This is not
232 entirely problematic, as the binding energy of these complexes is usually too weak for sensitive detection
233 even at the weakest transfer conditions. For typical analytes with moderate binding energies (e.g., iodide-
234 formic acid adducts), no significant declustering is observed at RF amplitudes $<125 V_{p-p}$. We find that the
235 optimal voltage gradients in the first quadrupole region are typically all 0 V between electrodes, as ions are
236 focused on the radial direction efficiently by the RF but transported axially by the gas flow. This ensures
237 that ions are transmitted with the lowest possible added energy into the next stage of the vacuum interface.
238 The rest of the differentially pumped interface is pumped by a single split flow turbo pump (Pfeiffer SF270)
239 and consists of an additional segmented quadrupole ion guide held at 10^{-2} mbar which transfers
240 energetically cooled ions into a lens stack held at 10^{-5} mbar before an orthogonal extraction in a time-of-
241 flight mass analyzer (Tofwerk Vocus CI-TOF 2R) operated at $<10^{-6}$ mbar. The instrument was configured
242 to measure a mass-to-charge (m/Q) range of 1–900 Th (12 kHz extraction frequency) with a mass resolving
243 power of 10 000 – 11 000 for the experiments described herein.



244 2.5 Flow Tube Oxidation Experiments

245 Ozonolysis/OH radical initiated oxidation of α -pinene ($C_{10}H_{16}$) experiments were performed under dry
246 conditions, at room temperature and atmospheric pressure in a flow tube reactor. The reactor consisted of
247 a ~ 6-litre Pyrex glass tube (80 mm i.d., \times 120 cm length). The total flow rate of dry synthetic air (N_2/O_2
248 80:20) was set at 5.5 slpm giving an average residence time of 70 seconds. Mixing ratio of 60 -70 ppb of
249 ozone generated by an ozone generator (Fisher Scientific, SOG-1) was continuously injected into the flow
250 tube. A mixing ratio of 200 ppb α -pinene was introduced from a homemade gas cylinder (40 ppm in UHP
251 N_2). The sample was immediately sampled into the reactor at a sample flow rate of 1.8 slpm with the excess
252 flow going to exhaust.

253 2.6 Calibration

254 To measure the instrument's sensitivity, we calibrated the reactor using different compounds each selected
255 to follow general structural selectivity rules for each ion chemistry. For example, no sensitivity for xylene
256 is reported for negative ions, as negative ions like iodide do not detect xylene with any significant
257 sensitivity. To calibrate benzene cations, we used a multicomponent gas (Apel Riemer Environmental Inc)
258 containing a mixture of hydrocarbons and ketones (Table S1). An internal calibration gas system consisting
259 of two mass flow controllers (Bronkhorst, capacity 30 and 2000 sccm) and a mixing volume diluted a flow
260 of 10 sccm of the gas standard into a carrier flow of 2000 sccm of UHP nitrogen resulting in a final mixing
261 ratio for each compound present in the gas mixture of 5 ppb. For iodide anions and protonated acetone
262 dimers, a liquid calibration system (LCS v2, Tofwerk) was used to form standard concentrations of lower
263 volatile species not compatible with gas cylinders. By introducing a continuous flow of liquid with known
264 concentration into a nebulizer and aluminum evaporation chamber, the LCS provides a continuous,
265 calibrated gas-phase concentration to the instrument. The evaporation chamber of the LCS was set to a
266 temperature of 150 °C, with a UHP nitrogen flow rate of 2000 slpm thereby slightly overflowing the sample
267 inlet. For the lower volatility compounds, we cannot rule out losses in the LCS, but find that collision-
268 limited sensitivities between positive and negative ion modes agree well within experimental uncertainty.



269 Aqueous solutions with concentrations ranging from 5 to 50 μM , and liquid flow rates of 10 $\mu\text{L}/\text{min}$, were
270 used to reach target concentrations in the low ppb range for each molecule and maintain constant water
271 vapor concentrations during calibration. Ammonia concentrations were generated using a gas standard and
272 independently compared to a cavity ring-down spectroscopy gas analyzer (Picarro Model G2508) to
273 validate the sensitivity and linearity of protonated acetone dimers towards ammonia (Figure S2).

274 Instrument backgrounds and detection limits are determined by measuring UHP nitrogen at the entrance
275 of the reactor. We note that measuring the total background should include any background measurement
276 of sampling inlets, but such characterization and best practices for sampling is beyond the scope of this
277 paper and discussed in detail elsewhere (Palm et al., 2019; Riva et al., 2019). We therefore report detection
278 limits using UHP nitrogen overflowing the inlet by using the zero port which introduces zero gas just to the
279 high-pressure (atmosphere) side of the critical orifice at the entrance of the reactor. We purged the
280 instrument before and after the calibration experiment for ten minutes with UHP nitrogen to determine the
281 instrument background count rates. As reported in detail previously (Palm et al., 2019), during a background
282 measurement the reactor walls are pushed out of equilibrium by the incoming clean air. This perturbation
283 can impart a transient effect on different compounds depending on primarily volatility. For volatile and
284 extremely low volatile compounds the response to a step change in concentration (introduction of zero air)
285 is close to instantaneous (< 100 ms) due to negligible adsorption (sticking rate), for the volatile species and
286 effectively infinitely slow evaporation rates from walls for the lowest volatility compounds (irreversible
287 loss). For background determinations the most challenging group of compounds are intermediate and semi-
288 volatile compounds which readily respond to changing inlet conditions and partition back and forth between
289 the reactor walls and the reactor flow. In laboratory conditions or at ground sites where temporal changes
290 are often only slowly changing, we use dry UHP N_2 to replace the incoming sample air for 1 minute. As
291 noted in prior work, under more dynamic environments the duration and frequency of instrument
292 background measurements should be decreased and increased respectively to match the temporal changes
293 which are to be measured.



294 3. Results and discussion

295 3.1. Vocus AIM time response

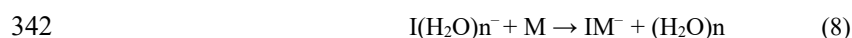
296 Real time measurements require fast time response to report temporal trends in measured concentrations
297 accurately. For many compounds, the time response can approach that of the volumetric time response of
298 the reactor (3 ~ 30 ms), however for semi-volatile (i.e., sticky) compounds the time response is often
299 observed to be much slower than the volumetric time constant as interaction with the reactor walls results
300 in smearing of the concentration over time. The primary interaction of the analyte and the reactor walls
301 defines the response time at constant temperature, pressure, and flow. Therefore, optimizing the shape and
302 the materials of the wetted surfaces is critical to maintaining a fast response. The Vocus AIM reactors'
303 conical design notably improves the time response by ensuring that the walls get further and further from
304 the exit orifice along the length of the reactor. This shape increases the probability that vapors that have
305 interacted with the wall are pumped away instead of being ionized and transferred into the mass analyzer.
306 It also ensures that in the region of the primary expansion, the recirculation eddies do not have significant
307 space to form, allowing a faster equilibration time at the entrance of the reactor (Figure 1). To accurately
308 measure dynamic changes in concentration, particularly for low-volatility species like oxidized organics,
309 inorganic acids, and reactive species, cPTFE is chosen as the reactor wall material. Teflon® based materials
310 have on average the weakest interaction with most organic and inorganic compounds (Morris et al., 2023)
311 and are therefore a good choice for the reactor walls. cPTFE in particular is chosen as its conductivity
312 prevents surface charge-up of the reactor walls which would result in unstable or slowly equilibrating ion
313 signals. We evaluate the performance of the reactor using molecules that represent a worst-case scenario
314 i.e., have a high surface affinity and interact strongly with the walls of the reactor. In Figure 2 we compare
315 the measurement of nitric acid in the AIM reactor with iodide adduct ionization with other IMR reactors
316 (Lee et al., 2018; Palm et al., 2019) with different approaches to improve the time response, notably a very
317 short stainless steel tubular reactor, and a larger flow tube reactor with laminarizer and sheath flow operated
318 at reduced pressure. To quantitatively compare the time responses of these different reactors we measured



319 the decay time, defined as the duration for the signal to fall below 90% of its peak value after the source of
320 nitric acid is removed. While the response time of the Vocus AIM reactor is not instantaneous, it is roughly
321 a factor of 3-4 faster than previously published medium pressure reactors. The improved time response is
322 most critical for ensuring that the memory effect in the reactor is minimized, crucial for applications where
323 fast transients need to be quantified, for example in mobile laboratories, aircraft, or flow tube reactors.

324 3.2 Water Vapor Control and Suppression.

325 A major limitation of chemical ionization reactors operated at elevated pressure is that water vapor can
326 strongly impact the net reaction mechanism and reagent ion distribution resulting in sensitivities that are
327 humidity-dependent (Zhang W. et al., 2023; Zhang Y. et al., 2023) as shown in Figure S3 for the reagent
328 ion distribution. Such changes pose considerable challenges for accurate quantification of species in
329 conditions where humidity is variable. The sensitivity to a given compound will depend on whether water
330 vapor competes with it for the reagent ion, i.e., lowering the sensitivity, or whether the presence of water
331 molecule offers a loosely bound third body to stabilize the adduct by removing the excess energy after the
332 {M-(reagent ion)} collision, thereby increasing sensitivity. While post measurement correction can be
333 performed, it is labor-intensive and prone to errors as each compound has essentially a unique humidity
334 dependence. To overcome this fundamental drawback, the Vocus AIM reactor introduces a system to
335 mitigate water vapor dependencies using a dopant. The dopant effectively replaces water vapor, the
336 dominant ligand in the switching reaction involving the reagent ions and the analyte molecules. A dopant
337 could in principle be any molecule that binds (forms an adduct) with the reagent ion more strongly than the
338 reagent ion and water. In this way, the dopant can displace the water molecules that would normally be
339 attached to the reagent ions with a compound that is not variable or present in significant concentrations in
340 the sample gas. The following equations show the modified reaction mechanism in the presence of a dopant
341 (D) in the case of iodide anions.





344 The modified reaction mechanism no longer significantly depends on varying water vapor conditions as
345 long as the dopant molecule is present in sufficiently high concentrations to replace most of the water
346 ligand. In the above chemical ionization mechanism for iodide anions, the challenge can be to choose a
347 suitable dopant. While the dopant must efficiently displace the water that is bound to iodide, it is also
348 desirable for the binding energy to be close to that of water. This ensures that the net chemical ionization
349 selectivity remains nearly unchanged compared to the dopant-free conditions. If a dopant with a very high
350 binding energy is selected, it will introduce a binding energy ionization threshold which will significantly
351 change the selectivity of the given ion chemistry by essentially removing all weakly bound adducts from
352 the spectra. Here we investigate three different dopants including acetonitrile, methanol, and acetone. These
353 compounds weakly interact with iodide anions and have a high vapor pressure which facilitates their easy
354 introduction into the reactor. This is typically achieved using a mass flow controller (Bronkhorst Low Delta
355 P, 30 sccm MFC) that draws from the headspace of a liquid reservoir, effectively minimizing the net dilution
356 (net sample dilution ~1%).

357 For each of the evaluated dopants, stable concentrations of formic, nitric, and acrylic acids were
358 introduced into the entrance of the reactor. The incoming air was humidified with two mass flow controllers,
359 one delivering dry nitrogen and the other passing dry nitrogen through a water bubbler held at room
360 temperature. The ratio of the two mass flow controllers was programmatically changed to simulate changes
361 in sample humidity for each dopant flow rate. Figure 3 illustrates how the systematic introduction of each
362 of these dopants at different mass flow rates influences the reactor's detection efficiency for nitric, formic,
363 and acrylic acids under changing humidity levels (0 - 100% relative humidity at 25°C). These compounds
364 were selected as characteristic compounds for the iodide adduct system, each demonstrating a distinct
365 sensitivity dependence on humidity which follows the changes in the water-iodide cluster distribution (Lee
366 et al., 2014).

367 Under dopant-free conditions, we expect nitric acid to first sharply increase from dry conditions to
368 humid conditions followed by a plateau at water vapor partial pressures of ~0.25 mbar. This can be
369 attributed to nitric acid's high binding enthalpy with I^- and a small, (1kcal/mol), difference to the binding



370 enthalpy to $I(H_2O)^-$ that is sufficiently compensated by the kinetic stabilization from the increased number
371 of vibrational modes due to the addition of the water molecule (Lopez et al., 2016). In the case of acrylic
372 acid, the sensitivity as a function of water vapor concentration falls rapidly following the availability of
373 unhydrated iodide anions. With increasing water vapor concentrations, the weak binding energy between
374 acrylic acid is not enough to overcome the competition with water for the bare iodide ions. Formic acid is
375 between these two extremes, initially stabilized by the presence of water, but ultimately in competition with
376 water for iodide ions as the second water cluster forms reducing the sensitivity at higher absolute humidity.

377 In the doped conditions, the humidity dependencies are significantly reduced for all molecules. The
378 dopant and humidity scans demonstrate the net effect of the different dopants for each molecule as a
379 function of the total dopant flow introduced. While methanol and acetone to a certain extent shift the reagent
380 ion distribution, they are not present in high enough concentrations to fully displace the water and stabilize
381 the reagent ion distribution against changes driven by humidity changes. Acetonitrile on the other hand
382 demonstrates a significant shift in reagent ion distributions and a significant damping of the humidity
383 dependency, particularly at flows greater than ~ 20 sccm. With acetonitrile as the dopant, the change in
384 sensitivity across the humidity range is reduced to a deviation of $<20\%$ relative to dry conditions for all
385 model compounds, more for formic acid and nitric acid ($<XX\%$). From the relative flattening of the
386 humidity dependence, for iodide anions (Caldwell et al., 1989) acetonitrile emerges as the most efficient
387 dopant tested reducing sensitivity variability across most analytes to a deviation that becomes negligible
388 for ambient analysis.

389 While this example focused on the dopant's presence in the reaction mechanism for iodide anions,
390 the same concept holds for any adduct forming ion including Br^- and Cl^- . For example, when generating
391 protonated ammonium ions in the presence of acetone, the formation of the $C_3H_6O-NH_4^+$ adduct with
392 acetone itself acts as a dopant and greatly suppresses the water vapor dependency, as demonstrated in Figure
393 S4. Where ammonium ions alone exhibit order of magnitude humidity dependencies when operated at
394 elevated pressure, this variability is reduced to $<30\%$ with significant acetone present as the dopant
395 (Canaval et al., 2019; Xu et al., 2022; Li et al., 2023), greatly simplifying analysis.



396 3.3 Sensitivity and Limits of Detection

397 Sensitivities for a variety of compounds were evaluated for each ion chemistry to quantify the overall
398 instrument performance. Calibrations were typically done at one or two different concentration steps in the
399 range of a few ppbv. Sensitivities were normalized to the number of recorded reagent ions measured at the
400 detector, which provides a straightforward method for correcting for any absolute fluctuations in the
401 instrument's response over time and referenced to a recorded total reagent ion current of 10^6 ions/second.
402 Typical reagent ion currents measured on the Vocus AIM reactors are between $3 - 6 \times 10^6$ ions/second for
403 iodide anions and benzene cations. Results from the calibration experiments are summarized in Table 1
404 organized by reagent ion. The compounds for calibration were specifically selected based on their
405 selectivity for each reagent ion and their relative ease of producing stable concentrations. A diverse range
406 of hydrocarbons, reactive nitrogen species, organic compounds (with various volatilities), and inorganic
407 acids can be detected with high sensitivities often greater than ~ 10 cps/ppt/ 1×10^6 RI. The sensitivity of
408 the Vocus AIM reactor does not necessarily surpass that of previous low and medium-pressure reactors
409 (Lee et al., 2014, 2018; Ye et al., 2021; Xu et al., 2022) in an absolute sense, however, the sensitivity is in
410 the same approximate range and reaches the extremely low limit of detections (LoD) ranging from 0.1 to 5
411 ppt for most compounds. An example, using acetone dimers as reagent ions, the LoD for ammonia is about
412 10 ppt (1 min averaging), which is 1-8 times lower than previously reported for this compound (You et al.,
413 2014; Dong et al., 2022; Schobesberger et al., 2022). Additionally, using a benzene cation as a reagent ion,
414 the LoD for monoterpenes (e.g., 0.2 ppt for α -pinene at 1 min) can even surpass conventional PTR
415 techniques, including the Vocus PTR (i.e., 4 ppt for α -pinene at 1 min; Krechmer et al., 2018) and similar
416 to the FUSION PTR (i.e., 0.1 pptv for 1 minute;).

417 The absolute sensitivity of the instrument depends fundamentally on the reaction time and collision
418 frequency (pressure) as well as the absolute number of generated reagent ions introduced into the reactor.
419 Figure 4a shows the dependence of the measured sensitivity of levoglucosan on the reactor pressure. By
420 increasing the pressure from 35 to 75 mbar the sensitivity of the instrument can be increased by a factor of



421 ~ 4 which is consistent with the increase expected based on reaction time and collision frequency. Operating
422 at higher pressures can be beneficial in pristine or highly diluted environments, where the concentrations
423 of target compounds can reside in the sub-parts-per-trillion (sub-ppt) range. A nominal operation pressure
424 of 50 mbar provides a good balance between sensitivity and linear range which under typical conditions
425 extends to ~100-200 ppbv depending on the analyte (Figure 4b). This allows the standard conditions (which
426 are a compromise between sensitivity and linear range) of the Vocus AIM reactor to operate equally well
427 in pristine and polluted environments with the same configuration. In highly polluted environments where
428 the total detectable mass concentrations greatly exceed the linear range of the instrument, reagent ion
429 normalization can compensate for up to 50% of reagent ion depletion before normalization errors begin to
430 accumulate. In such conditions, the incoming sample flow would need to be diluted, to maintain
431 concentrations within the normalization range.

432 Finally, taking advantage of the improved time response and the possibility of operating more than
433 one VUV lamp on the Vocus AIM reactor (Figure 1), a fast switch between different ion chemistries at up
434 to 2 Hz is now possible as shown in Figure S5. This valuable feature allows the Vocus AIM reactor to
435 extend the variety of compounds detected by one instrument within a single polarity, as the mass analyzer
436 used in this study had polarity switching timescales of 5-10 minutes.

437 3.4 Vocus AIM Performance for Atmospheric Applications

438 To evaluate the bulk detection capabilities of Vocus AIM we measured oxidation products from the OH/O₃
439 initiated oxidation of α -pinene using a steady-state flow tube setup. This reaction mechanism was chosen
440 because it is a well-studied system resulting in a suite of oxidation products spanning a wide range of
441 functionalities. Additionally, it generates molecules with a wide range of molecular masses, from lightly
442 oxidized monomers to heavily oxidized dimers. In total, four AIM reagent ion chemistries, namely NH₄⁺,
443 Cl⁻, I⁻ and NO₃⁻ were used to investigate their relative detection efficiency (selectivity) towards produced
444 OVOCs. AIM offers an ideal method for evaluating ion chemistries as it ensures uniformity in the
445 introduction of all reagent ions and utilizes the same analytical instrument for comparison. This approach



446 effectively eliminates the instrument-to-instrument variability, thus providing a highly direct and unbiased
447 comparison of ion chemistry and detection efficacy for a variety of mixed organic compounds.

448 The formation of RO₂ radicals generated from the combined ozonolysis and OH radical reaction of
449 α-pinene can further react forming mixed oxidation products during the reaction time in the flow tube.
450 Among the different RO₂ radicals formed, C₁₀H₁₅O_{>3} and C₁₀H₁₇O_{>2} were detected by the different reagent
451 ions used. While the mass spectra are generally similar between the different reagent ion chemistries, there
452 are some notable differences in the detection efficiencies. NO₃⁻ ion-based chemistry is by far the most
453 selective of the reagent ions tested. A smaller group of compounds was detected, with a particular
454 inclination towards the most heavily oxidized monomers and gas-phase dimer species. The variable
455 selectivity of the different ion chemistries is demonstrated in Figure 5, organized by the increase of reagent
456 ion selectivity. NH₄⁺ and Cl⁻ are the least selective ions evaluated, highlighted by the large ion signal
457 intensity of compounds m/Q < 100 Th (least oxidized) and the largest number of absolute compounds
458 detected. While the sensitivity towards less oxidized compounds is limited to the less selective reagent ions
459 (i.e., NH₄⁺ and Cl⁻), more selective reagent ions excel at detecting the lower concentration of more oxidized
460 compounds. The selectivity of the reagent ion plays a pivotal role in limiting the backgrounds and potential
461 isobaric interferences that might hamper the detection of the compounds of interest. With the AIM reactor
462 and the right selection of reagent ion, even the highest oxidized RO₂ radicals (e.g., C₁₀H₁₇O₇ and C₁₀H₁₅O₈),
463 and dimeric products (e.g., C₁₉H_{28,30}O_x C₂₀H_{30,32}O_x) can be identified under relevant atmospheric conditions,
464 highlighting the very high sensitivity and versatility of the Vocus AIM reactor.

465 To demonstrate the bulk detection properties of the different reagent ion chemistries more clearly,
466 we categorized each compound according to its estimated volatility. Due to the lack of authentic standards
467 measuring the vapor pressure of oxygenated organic molecules (OOMs) remains an analytical challenge.
468 To overcome this problem, model calculations have been developed to estimate the vapor pressure using,
469 for example, structure-based estimations and formula-based estimations. The volatility basis set (VBS)
470 framework has been established by Donahue et al. (2011) and is widely used in atmospheric chemistry to
471 estimate the volatility of products measured by mass spectrometry techniques. The VBS parameterization



472 is useful for classifying the wide range of OOMs into multiple volatility groups, including extremely low
473 volatility organic compounds (ELVOC) and low volatility organic compounds (LVOC) based on their
474 effective saturation concentration (C^*) in the unit of $\mu\text{g m}^{-3}$. In this work, we apply the VBS
475 parameterization optimized by Li et al. (2016),

$$476 \quad \log_{10}C^*(298K) = (n_C^0 - n_C)b_C - n_O b_O - 2 \frac{n_C n_O}{(n_C + n_O)} b_{CO} - n_N b_N - n_S b_S \quad (10)$$

477

478 where n_C , n_O , n_N , and n_S are the number of carbon, oxygen, nitrogen, and sulfur atoms of the specific
479 molecule, separately; n_C^0 is the reference carbon number; b_C , b_O , b_N , and b_S are the contribution of each
480 atom to $\log_{10}C^*$, respectively; b_{CO} is the carbon-oxygen nonideality. The b coefficient values can be found
481 in Li et al. (2016). In this study, all oxidation products generated from the OH/O₃ initiated oxidation were
482 grouped into six volatility regimes; ultralow-volatility (ULVOCs, $C^* < 10^{-8.5} \mu\text{g m}^{-3}$), extremely low
483 volatility (ELVOCs, $10^{-8.5} < C^* < 10^{-4.5} \mu\text{g m}^{-3}$), low-volatility (LVOCs, $10^{-4.5} < C^* < 10^{-0.5} \mu\text{g m}^{-3}$), semi-
484 volatile (SVOCs, $10^{-0.5} < C^* < 10^{2.5} \mu\text{g m}^{-3}$), intermediate-volatility organic compounds (IVOC, $10^{2.5} < C^*$
485 $< 10^{6.5} \mu\text{g m}^{-3}$), and VOC ($10^{6.5} < C^* \mu\text{g m}^{-3}$) based on VBS.

486 Figure 6 illustrates the measured range of oxidation products generated by the hydroxyl radical and
487 ozone reaction with α -pinene. These products were analyzed using one mass spectrometer with AIM reactor
488 setup employing various ionization chemistries. Therefore, unlike other studies (Riva et al., 2019, Li et al.,
489 2023) this study utilizes a single instrument, thereby reducing uncertainties associated with the calibration
490 and settings of different instruments as well as the conditions during sample collection. The total signal in
491 each volatility bin represents the sum of the signal intensity of OOMs within the volatility range. Organic
492 compounds with C^* of $< 10^{-1} \mu\text{g m}^{-3}$ made up the largest signal contributions for the Vocus AIM using
493 NO₃⁻-ion based chemistry (Table S2). This observation is consistent with the conventional atmospheric
494 pressure using NO₃⁻ as the reagent ion and indicates that the design of the Vocus AIM reactor allows the
495 detection of ELVOC and ULVOC (Riva et al., 2019; Zhang W. et al., 2023; Zhang Y. et al., 2023). This is
496 a substantial improvement for the atmospheric science community as measurement of such species is solely



497 possible with the use of atmospheric pressure interfaces which can be associated with sensitivity
498 fluctuations (e.g., RH effect). As demonstrated previously (Riva et al., 2019), I⁻-ion based chemistry detects
499 oxygenated compounds with C* ranging from 10⁻⁵ to 10⁵ µg m⁻³ which corresponds to OOMs and start
500 being less sensitive to oxygenated compounds having fewer oxygen atoms and are included in the IVOC
501 fraction. While Cl⁻ and NH₄⁺ can also measure OOM with C* as low as 10⁻⁵ µg m⁻³ the weak selectivity of
502 these ion-based chemistries allows them to measure a wider range of compounds (i.e., IVOCs and VOCs).
503 IVOCs and VOCs generally include less oxygenated VOCs with shorter carbon skeletons and comprise the
504 main fraction of organics formed from the oxidation of pinene (Isaacman-VanWertz et al., 2018). We stress
505 here that while it was not possible to detect ULVOC and ELVOC using I⁻, Cl⁻, NH₄⁺-ion based chemistries
506 it is purely a selectivity limitation of the more general reagent ions not of absolute sensitivity as all the
507 tested reagent ions have similar overall absolute sensitivities. Nitrate reagent ions benefit from the high
508 selectivity, which also manifests in a lower background signal therefore enabling nitrate anion chemistry to
509 detect ULVOC and ELVOC. With the significantly lower background concentrations of nitrate ions, the
510 detection of compounds at extremely low concentrations (as low as 10-100 ppqv) becomes possible.

511 Differences in the contribution of these compound groups with previous work could be due to
512 different sensitivities of the instruments towards organic compounds with varying oxidation extents (Riva
513 et al., 2019). By carefully selecting the type of reagent ion, the combined volatility distribution can cover
514 from VOCs to OOMs, with varying O:C ratios and volatility ranges (Figure 6) all within a single instrument.
515 The Vocus AIM can therefore provide a more complete picture of the volatility distribution of gaseous
516 organic and inorganic compounds found in the atmosphere.

517 Conclusions

518 The primary goal of this work was to evaluate the performance of the newly designed Vocus AIM reactor
519 to determine the time response, sensitivity, and selectivity using multiple reagent ions. Of specific
520 importance, we introduced and demonstrated the utility of a dopant-based water vapor suppression system
521 which improves data quality and reduces the number of corrections required during analysis. By comparing



522 detection efficiency for different compounds, we demonstrated that the Vocus AIM captures nearly the
523 entire range of OVOC, spanning from VOC to ULVOC by using different types of reagent ions. Through
524 the optimization of reactor geometry and materials, the time response of the Vocus AIM reactor is greatly
525 improved even for sticky and reactive compounds. The high sensitivity achieves sub-ppt detection limits
526 for a range of VOCs and VICs. The innovative design of the new reactor substantially eliminated this
527 humidity sensitivity, facilitating more straightforward measurements of samples with water vapor and
528 simplifying data interpretation. This improvement is crucial for robust and reliable analysis across a
529 spectrum of environmental samples. As a result, the Vocus AIM reactor represents a highly versatile
530 platform able to measure the wide variety of VOCs and VICs in the atmosphere using a single instrument.
531



532 **Conflicts of interest**

533 All (co-)authors, except S.P. and J.A.T. work for Tofwerk AG, which is commercializing the
534 Vocus-AIM mass spectrometer.

535 **Author Contributions**

536 M.R., V.P., F.L., conceive the study. M.R., V.P., C.F., P.B., S.P., S.J., and F.L. collected and
537 analyzed the data. P.S., U.R., and F.L. conceived the design of the Vocus AIM reactor. M.R., V.P.,
538 F.L. wrote the manuscript. All authors discussed the results and commented on the paper.

539

540 **Acknowledgements:**

541 We would also like to thank Withtech Inc, and Minji Park for providing calibration comparison
542 data with the Picarro CRDS.

543

544 **References**

- 545 Berndt, T., Richters, S., Kaethner, R., Voigtlander, J., Stratmann, F., Sipila, M., Kulmala, M., and
546 Herrmann, H.: Gas-Phase Ozonolysis of Cycloalkenes: Formation of Highly Oxidized RO₂ Radicals and
547 Their Reactions with NO, NO₂, SO₂, and Other RO₂ Radicals, *J. Phys. Chem. A*, 119, 10336-10348,
548 10.1021/acs.jpca.5b07295, 2015.
- 549 Berndt, T., Herrmann, H., and Kurten, T.: Direct Probing of Criegee Intermediates from Gas-Phase
550 Ozonolysis Using Chemical Ionization Mass Spectrometry, *J. Am. Chem. Soc.*, 139, 13387-13392,
551 10.1021/jacs.7b05849, 2017.
- 552 Berndt, T., Mentler, B., Scholz, W., Fischer, L., Herrmann, H., Kulmala, M., and Hansel, A.: Accretion
553 Product Formation from Ozonolysis and OH Radical Reaction of alpha-Pinene: Mechanistic Insight and
554 the Influence of Isoprene and Ethylene, *Environ. Sci. Technol.*, 52, 11069-11077,
555 10.1021/acs.est.8b02210, 2018.
- 556 Bertram, T. H., Kimmel, J. R., Crisp, T. A., Ryder, O. S., Yatavelli, R. L. N., Thornton, J. A., Cubison, M.
557 J., Gonin, M. and Worsnop, D. R.: A field-deployable, chemical ionization time-of-flight mass
558 spectrometer, *Atmos. Meas. Tech.*, 4(7), 1471–1479, doi:10.5194/amt-4-1471-2011, 2011.
- 559 Bianchi, F., Kurten, T., Riva, M., Mohr, C., Rissanen, M. P., Roldin, P., Berndt, T., Crouse, J. D.,
560 Wennberg, P. O., Mentel, T. F., Wildt, J., Junninen, H., Jokinen, T., Kulmala, M., Worsnop, D. R.,
561 Thornton, J. A., Donahue, N., Kjaergaard, H. G., and Ehn, M.: Highly Oxygenated Organic Molecules
562 (HOM) from Gas-Phase Autoxidation Involving Peroxy Radicals: A Key Contributor to Atmospheric
563 Aerosol, *Chem. Rev.*, 119, 3472-3509, 10.1021/acs.chemrev.8b00395, 2019.
- 564 Breitenlechner, M., Fischer, L., Hainer, M., Heinritzi, M., Curtius, J., and Hansel, A.: PTR3: An Instrument
565 for Studying the Lifecycle of Reactive Organic Carbon in the Atmosphere, *Anal. Chem.*, 89, 5824-5831,
566 10.1021/acs.analchem.6b05110, 2017.



- 567 Breitenlechner, M., Novak, G. A., Neuman, J. A., Rollins, A. W., and Veres, P. R.: A versatile vacuum
568 ultraviolet ion source for reduced pressure bipolar chemical ionization mass spectrometry, *Atmos. Meas.*
569 *Tech.*, 15, 1159–1169, <https://doi.org/10.5194/amt-15-1159-2022>, 2022.
- 570 Bruderer, T., Gaisl, T., Gaugg, M.T., Nowak, N., Streckenbach, B., Müller, S., Moeller, A., Kohler, M.,
571 and Zenobi, R.: On-Line Analysis of Exhaled Breath, *Chem. Rev.*, 119, 19, 10803–10828,
572 10.1021/acs.chemrev.9b00005, 2019.
- 573 Caldwell, G. W., Masucci, J. A., and Ikonomou, M. G.: Negative ion chemical ionization mass
574 spectrometry—binding of molecules to bromide and iodide anions, *Organic Mass Spectrometry*, 24, 8–
575 14, 10.1002/oms.1210240103, 1989.
- 576 Canaval, E., Hyttinen, N., Schmidbauer, B., Fischer, L., and Hansel, A.: NH_4^+ Association and Proton
577 Transfer Reactions With a Series of Organic Molecules, *Front. Chem.*, 7, 10.3389/fchem.2019.00191,
578 2019.
- 579 Crouse, J. D., Nielsen, L. B., Jørgensen, S., Kjaergaard, H. G., and Wennberg, P. O.: Autoxidation of
580 Organic Compounds in the Atmosphere, *J. Phys. Chem. Lett.*, 4, 3513–3520, 10.1021/jz4019207, 2013.
- 581 Donahue, N. M., Epstein, S. A., Pandis, S. N., and Robinson, A. L.: A two-dimensional volatility basis set:
582 I. organic-aerosol mixing thermodynamics, *Atmos. Chem. Phys.*, 11, 3303–3318, 10.5194/acp-11-3303-
583 2011, 2011.
- 584 Dong, F., Li, H., Liu, B., Liu, R., and Hou K.: Protonated acetone ion chemical ionization time-of-flight
585 mass spectrometry for real-time measurement of atmospheric ammonia, *J. Environ. Sci.*, 14, 66–74,
586 10.1016/j.jes.2021.07.023, 2022.
- 587 Ehn, M., Thornton, J. A., Kleist, E., Sipila, M., Junninen, H., Pullinen, I., Springer, M., Rubach, F.,
588 Tillmann, R., Lee, B., Lopez-Hilfiker, F., Andres, S., Acir, I. H., Rissanen, M., Jokinen, T.,
589 Schobesberger, S., Kangasluoma, J., Kontkanen, J., Nieminen, T., Kurten, T., Nielsen, L. B., Jørgensen,
590 S., Kjaergaard, H. G., Canagaratna, M., Maso, M. D., Berndt, T., Petaja, T., Wahner, A., Kerminen, V.
591 M., Kulmala, M., Worsnop, D. R., Wildt, J., and Mentel, T. F.: A large source of low-volatility secondary
592 organic aerosol, *Nature*, 506, 476–479, 10.1038/nature13032, 2014.
- 593 Eisele, F.L., Tanner, D.J., Measurement of the gas phase concentration of H_2SO_4 and methane sulfonic
594 acid and estimates of H_2SO_4 production and loss in the atmosphere, *J. Geophys. Res. Atmo.*, 98, 9001-
595 9010, 10.1029/93JD00031, 1993.
- 596 Hallquist, M., Wenger, J. C., Baltensperger, U., Rudich, Y., Simpson, D., Claeys, M., Dommen, J.,
597 Donahue, N. M., George, C., Goldstein, A. H., Hamilton, J. F., Herrmann, H., Hoffmann, T., Iinuma,
598 Y., Jang, M., Jenkin, M. E., Jimenez, J. L., Kiendler-Scharr, A., Maenhaut, W., McFiggans, G., Mentel,
599 T. F., Monod, A., Prévôt, A. S. H., Seinfeld, J. H., Surratt, J. D., Szmigielski, R., and Wildt, J.: The
600 formation, properties and impact of secondary organic aerosol: current and emerging issues, *Atmos.*
601 *Chem. Phys.*, 9, 5155–5236, 10.5194/acp-9-5155-2009, 2009.
- 602 Hansel, A., Scholz, W., Mentler, B., Fischer, L., and Berndt, T.: Detection of RO_2 radicals and other
603 products from cyclohexene ozonolysis with NH_4^+ and acetate chemical ionization mass spectrometry,
604 *Atmo. Environ.*, 186, 248–255, 10.1016/j.atmosenv.2018.04.023, 2018.
- 605 Isaacman-VanWertz, G. and Aumont, B.: Impact of organic molecular structure on the estimation of
606 atmospherically relevant physicochemical parameters, *Atmos. Chem. Phys.*, 21, 6541–6563,
607 10.5194/acp-21-6541-2021, 2021.
- 608 Ji, Y., Huey, L. G., Tanner, D. J., Lee, Y. R., Veres, P. R., Neuman, J. A., Wang, Y., and Wang, X.: A
609 vacuum ultraviolet ion source (VUV-IS) for iodide–chemical ionization mass spectrometry: a substitute
610 for radioactive ion sources, *Atmos. Meas. Tech.*, 13, 3683–3696, 10.5194/amt-13-3683-2020, 2020.
- 611 Krechmer, J., Lopez-Hilfiker, F., Koss, A., Hutterli, M., Stoermer, C., Deming, B., Kimmel, J., Warneke,
612 C., Holzinger, R., Jayne, J. T., Worsnop, D. R., Fuhrer, K., Gonin, M. and de Gouw, J. A.: Evaluation
613 of a New Reagent-Ion Source and Focusing Ion-Molecule Reactor for use in Proton-Transfer-Reaction
614 Mass Spectrometry, *Anal. Chem.*, 10.1021/acs.analchem.8b02641, 2018.
- 615 Lavi, A., Vermeuel, M. P., Novak, G. A., and Bertram, T. H.: The sensitivity of benzene cluster cation
616 chemical ionization mass spectrometry to select biogenic terpenes, *Atmos. Meas. Tech.*, 11, 3251–3262,
617 <https://doi.org/10.5194/amt-11-3251-2018>, 2018.



- 618 Lee, B. H., Lopez-Hilfiker, F. D., Mohr, C., Kurten, T., Worsnop, D. R., and Thornton, J. A.: An iodide-
619 adduct high-resolution time-of-flight chemical-ionization mass spectrometer: application to atmospheric
620 inorganic and organic compounds, *Environ. Sci. Technol.*, 48, 6309-6317, 10.1021/es500362a, 2014.
- 621 Lee, B. H., Lopez-Hilfiker, F. D., Veres, P.R., McDuffie, E.E., Fibiger, D.L., Sparks, T.M., Ebben, C.J.,
622 Green, J.R., Schroder, J.C., Campuzano-Jost, P., Iyer, S., D'Ambro, E.A., Schobesberger, S., Brown,
623 S.S., Wooldridge, P.J., Cohen, R.C., Fiddler, M.N., Bililign, S., Jimenez, J.L., Kurtén, T., Weinheimer,
624 A.J., Jaegle, L., and Thornton, J. A.: Flight Deployment of a High-Resolution Time-of-Flight Chemical
625 Ionization Mass Spectrometer: Observations of Reactive Halogen and Nitrogen Oxide Species, *J.*
626 *Geophys Res. Atmos.*, 123, 7670-7686, 10.1029/2017JD028082, 2018.
- 627 Li, Y., Pöschl, U., and Shiraiwa, M.: Molecular corridors and parameterizations of volatility in the chemical
628 evolution of organic aerosols, *Atmos. Chem. Phys.*, 16, 3327-3344, 10.5194/acp-16-3327-2016, 2016.
- 629 Li, D., Wang, D., Caudillo, L., Scholz, W., Wang, M., Tomaz, S., Marie, G., Surdu, M., Eccli, E., Gong,
630 X., Gonzalez-Carracedo, L., Granzin, M., Pfeifer, J., Rörup, B., Schulze, B., Rantala, P., Perrier, S.,
631 Hansel, A., Curtius, J., Kirkby, J., Donahue, N. M., George, C., El-Haddad, I., and Riva, M.: Ammonium
632 CI-Orbitrap: a tool for characterizing the reactivity of oxygenated organic molecules, *Atmos. Meas.*
633 *Tech. Discuss.* [preprint], <https://doi.org/10.5194/amt-2023-149>, in review, 2023.
- 634 Lopez-Hilfiker, F. D., Iyer, S., Mohr, C., Lee, B. H., D'Ambro, E. L., Kurtén, T. and Thornton, J.
635 A.: Constraining the sensitivity of iodide adduct chemical ionization mass spectrometry to
636 multifunctional organic molecules using the collision limit and thermodynamic stability of iodide ion
637 adducts, *Atmos. Meas. Tech.*, 9(4), 1505–1512, doi:10.5194/amt-9-1505-2016, 2016.
- 638 Mazzucotelli, M., Farneti, B., Khomenko, I., Gonzalez-Estanol, K., Pedrotti, M., Fragasso, M., Capozzi,
639 V., and Biasioli, F.; *Green Analytical Chemistry*, 3, 10.1016/j.greeac.2022.100041, 2022.
- 640 Morris, M. A., Pagonis, D., Day, D. A., de Gouw, J. A., Ziemann, P. J., and Jimenez, J. L.: Absorption of
641 VOCs by polymer tubing: implications for indoor air and use as a simple gas-phase volatility separation
642 technique, *EGUsphere* [preprint], <https://doi.org/10.5194/egusphere-2023-1241>, 2023.
- 643 Palm, B.P., Liu, X., Jimenez, X.L., and Thornton, J. A.: Performance of a new coaxial ion–molecule
644 reaction region for low-pressure chemical ionization mass spectrometry with reduced instrument wall
645 interactions, *Atmos. Meas. Tech.*, 12, 5829–5844, doi.org/10.5194/amt-12-5829-2019, 2019
- 646 Pfeifer, J., Simon, M., Heinritzi, M., Piel, F., Weitz, L., Wang, D., Granzin, M., Müller, T., Bräkling, S.,
647 Kirkby, J., Curtius, J., and Kürten, A.: Measurement of ammonia, amines and iodine compounds using
648 protonated water cluster chemical ionization mass spectrometry, *Atmos. Meas. Tech.*, 13, 2501–2522,
649 <https://doi.org/10.5194/amt-13-2501-2020>, 2020.
- 650 Reinecke, T., Leiminger, M., Jordan, A., Wisthaler, A., and Müller, M.: Ultrahigh Sensitivity PTR-MS
651 Instrument with a Well-Defined Ion Chemistry, *Anal. Chem.*, 95, 11879–11884,
652 <https://doi.org/10.1021/acs.analchem.3c02669>, 2023.
- 653 Rissanen, M. P., Mikkilä, J., Iyer, S., and Hakala, J.: Multi-scheme chemical ionization inlet (MION) for
654 fast switching of reagent ion chemistry in atmospheric pressure chemical ionization mass spectrometry
655 (CIMS) applications, *Atmos. Meas. Tech.*, 12, 6635-6646, 10.5194/amt-12-6635-2019, 2019.
- 656 Riva, M., Rantala, P., Krechmer, J. E., Peräkylä, O., Zhang, Y., Heikkinen, L., Garmash, O., Yan, C.,
657 Kulmala, M., Worsnop, D., and Ehn, M.: Evaluating the performance of five different chemical
658 ionization techniques for detecting gaseous oxygenated organic species, *Atmos. Meas. Tech.*, 12, 2403-
659 2421, 10.5194/amt-12-2403-2019, 2019.
- 660 Schobesberger, S., D'Ambro, E. L., Vettikkat, L., Lee, B. H., Peng, Q., Bell, D. M., Shilling, J. E.,
661 Shrivastava, M., Pekour, M., Fast, J., and Thornton, J. A.: Airborne flux measurements of ammonia over
662 the southern Great Plains using chemical ionization mass spectrometry, *Atmos. Meas. Tech.*, 16, 247–
663 271, <https://doi.org/10.5194/amt-16-247-2023>, 2023.
- 664 Tang, J., Schurgers, G., and Rinnan, R.; *Process Understanding of Soil BVOC Fluxes in Natural*
665 *Ecosystems: A Review*, *Rev. Geophys.*, 57, 966-986, 10.1029/2018RG000634, 2019.
- 666 Vasquez, K. T., Allen, H. M., Crouse, J. D., Praske, E., Xu, L., Noelscher, A. C., and Wennberg, P. O.:
667 Low-pressure gas chromatography with chemical ionization mass spectrometry for quantification of



- 668 multifunctional organic compounds in the atmosphere, *Atmos. Meas. Tech.*, 11, 6815–6832,
669 <https://doi.org/10.5194/amt-11-6815-2018>, 2018.
- 670 Xu, L., Coggon, M. M., Stockwell, C. E., Gilman, J. B., Robinson, M. A., Breitenlechner, M., Lamplugh,
671 A., Crouse, J. D., Wennberg, P. O., Neuman, J. A., Novak, G. A., Veres, P. R., Brown, S. S., and
672 Warneke, C.: Chemical ionization mass spectrometry utilizing ammonium ions (NH₄⁺ CIMS) for
673 measurements of organic compounds in the atmosphere, *Atmos. Meas. Tech.*, 15, 7353–7373,
674 <https://doi.org/10.5194/amt-15-7353-2022>, 2022.
- 675 Ye, C., Yuan, B., Lin, Y., Wang, Z., Hu, W., Li, T., Chen, W., Wu, C., Wang, C., Huang, S., Qi, J., Wang,
676 B., Wang, C., Song, W., Wang, X., Zheng, E., Krechmer, J.E., Ye, P., Zhang, Z., Wang, X., Worsnop,
677 D.R., and Shao, M.: Chemical characterization of oxygenated organic compounds in the gas phase and
678 particle phase using iodide CIMS with FIGAERO in urban air, *Atmos. Chem. Phys.*, 21, 8455–8478,
679 <https://doi.org/10.5194/acp-21-8455-2021>, 2021.
- 680 Yuan, B., Koss, A. R., Warneke, C., Coggon, M., Sekimoto, K., and de Gouw, J. A.: Proton-Transfer-
681 Reaction Mass Spectrometry: Applications in Atmospheric Sciences, *Chem. Rev.*, 117, 13187–13229,
682 [10.1021/acs.chemrev.7b00325](https://doi.org/10.1021/acs.chemrev.7b00325), 2017.
- 683 You, Y., Kanawade, V. P., de Gouw, J. A., Guenther, A. B., Madronich, S., Sierra-Hernández, M. R.,
684 Lawler, M., Smith, J. N., Takahama, S., Ruggeri, G., Koss, A., Olson, K., Baumann, K., Weber, R. J.,
685 Nenes, A., Guo, H., Edgerton, E. S., Porcelli, L., Brune, W. H., Goldstein, A. H., and Lee, S. H.:
686 Atmospheric amines and ammonia measured with a chemical ionization mass spectrometer (CIMS),
687 *Atmos. Chem. Phys.*, 14, 12181–12194, [10.5194/acp-14-12181-2014](https://doi.org/10.5194/acp-14-12181-2014), 2014.
- 688 Zhang, W., Xu, L., Zhang, H.: Recent advances in mass spectrometry techniques for atmospheric chemistry
689 research on molecular-level, *Mass Spectrom. Rev.*, 21857, [10.1002/mas.21857](https://doi.org/10.1002/mas.21857), 2023.
- 690 Zhang, Y., Liu, R., Yang, D., Guo, Y., Li, M., and Hou, K.: Chemical ionization mass spectrometry:
691 Developments and applications for on-line characterization of atmospheric aerosols and trace gases,
692 *Trends Anal. Chem.*, 168, [10.1016/j.trac.2023.117353](https://doi.org/10.1016/j.trac.2023.117353), 2023.
- 693

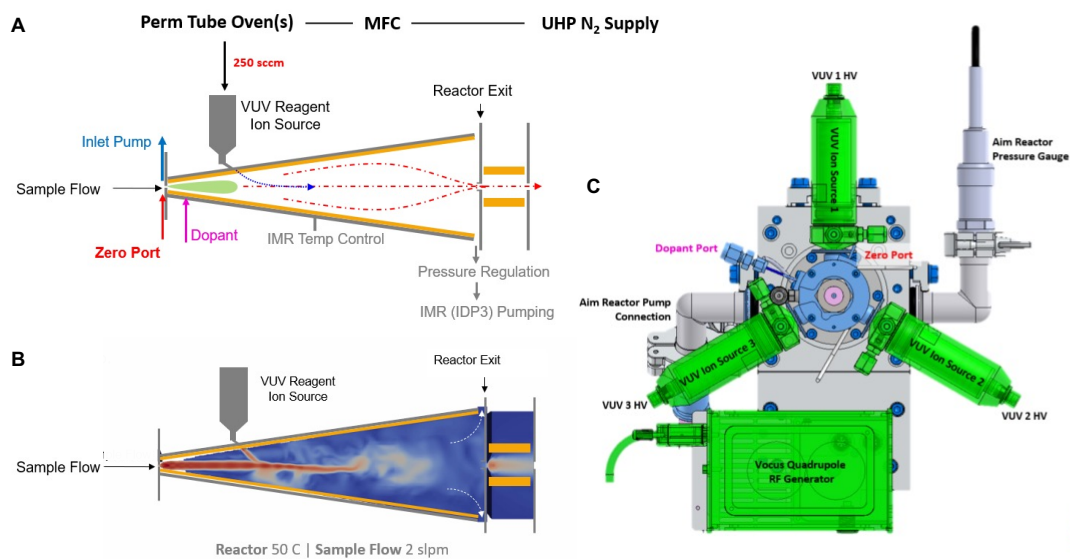


694 **Table 1.** Sensitivities (cps pptv⁻¹) normalized by 10⁶ detected reagent ions for different ion
695 chemistry used with the Vocus AIM reactor.
696

| Compounds | Reagent Ion | Sensitivity (cps/ppt/ 10 ⁶ ions/s) | LoD (1-min) |
|-------------------------|-------------------|--|----------------|
| toluene | Benzene (+) | 7.8 | 0.4 |
| m-xylene | Benzene (+) | 7.6 | 0.2 |
| 1,2,4-trimethyl benzene | Benzene (+) | 7.5 | 0.2 |
| α-pinene | Benzene (+) | 6.8 | 1.4 |
| ammonia | Acetone dimer (+) | 1.5 | 1 |
| methyl amine | Acetone dimer (+) | 1.2 | 10 |
| ethyl amine | Acetone dimer (+) | 1.6 | 1 |
| dimethyl amine | Acetone dimer (+) | 2.2 | 1 |
| diethyl amine | Acetone dimer (+) | 2.6 | 1 |
| trimethyl amine | Acetone dimer (+) | 2.5 | 4 |
| triethyl amine | Acetone dimer (+) | 5.0 | 2 |
| formic acid | Iodide (-) | 2.0 | 0.8 |
| levoglucosan | Iodide (-) | 6.0 | 0.1 |
| chlorine | Iodide (-) | 5.5 | 3 |
| nitric acid | Iodide (-) | 4.3 | 5 |
| fluoric acid | Iodide (-) | 3 | 10 |
| iodine | Bromide (-) | 3 | 2 |

697

698



699

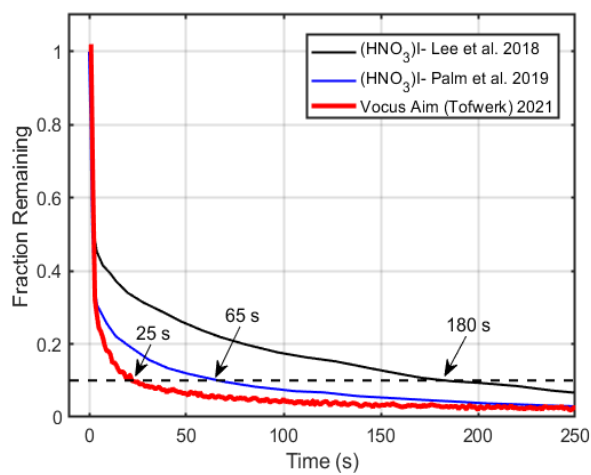
700 **Figure 1.** (A) Diagram of the Vocus AIM reactor showing the conical design and relative locations of the

701 sample and reagent ion addition. (B) Cross-sectional view of modeled flow velocities in the AIM-IMR,

702 showing optimized intersection of the reagent ion and sample stream flows, and limited contact of the

703 sample gas with surfaces. (C) Key components of the Vocus AIM reactor.

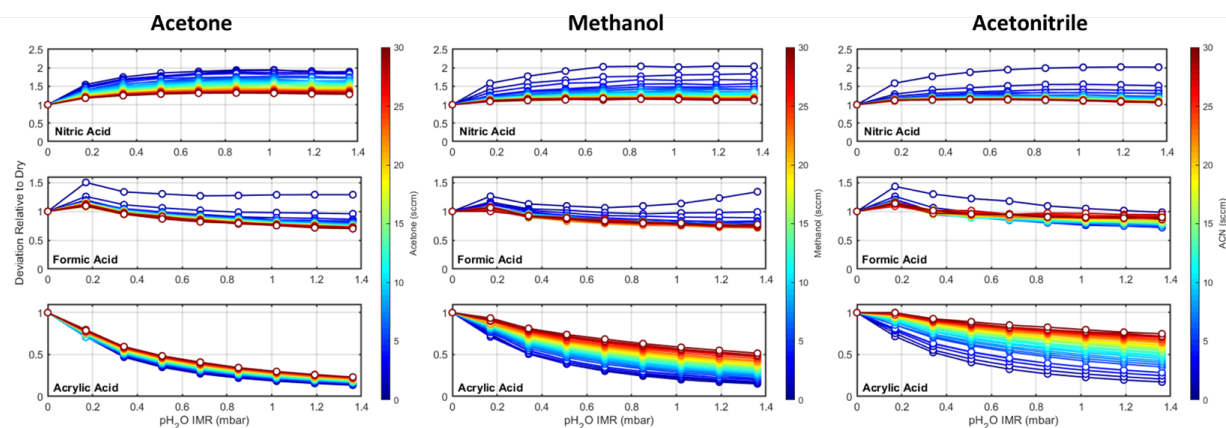
704



705

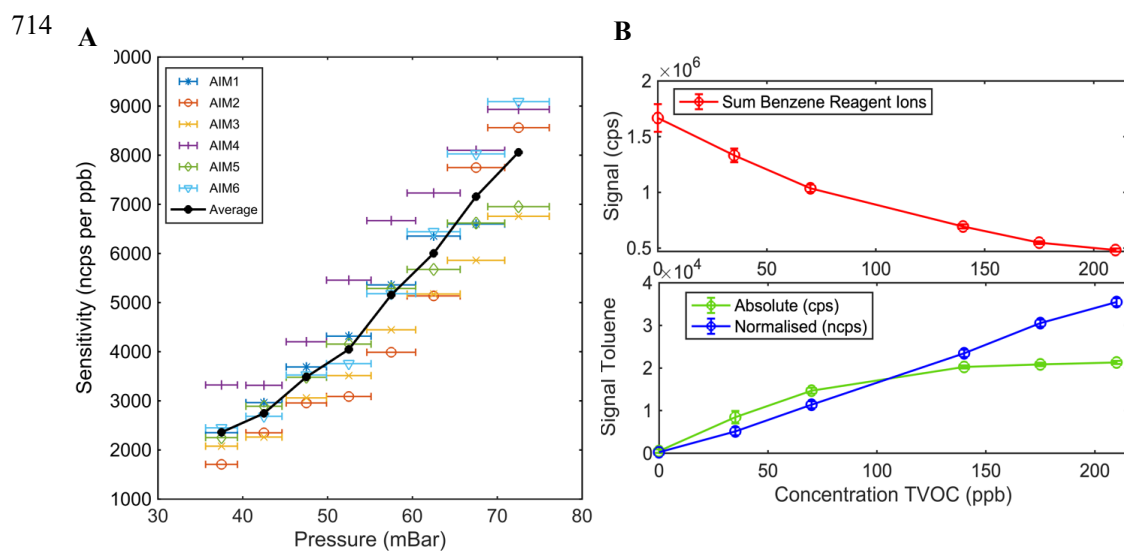
706 **Figure 2.** Time response to nitric acid of the Vocus AIM IMR compared to the previous IMR designs

707 found in the literature.



708

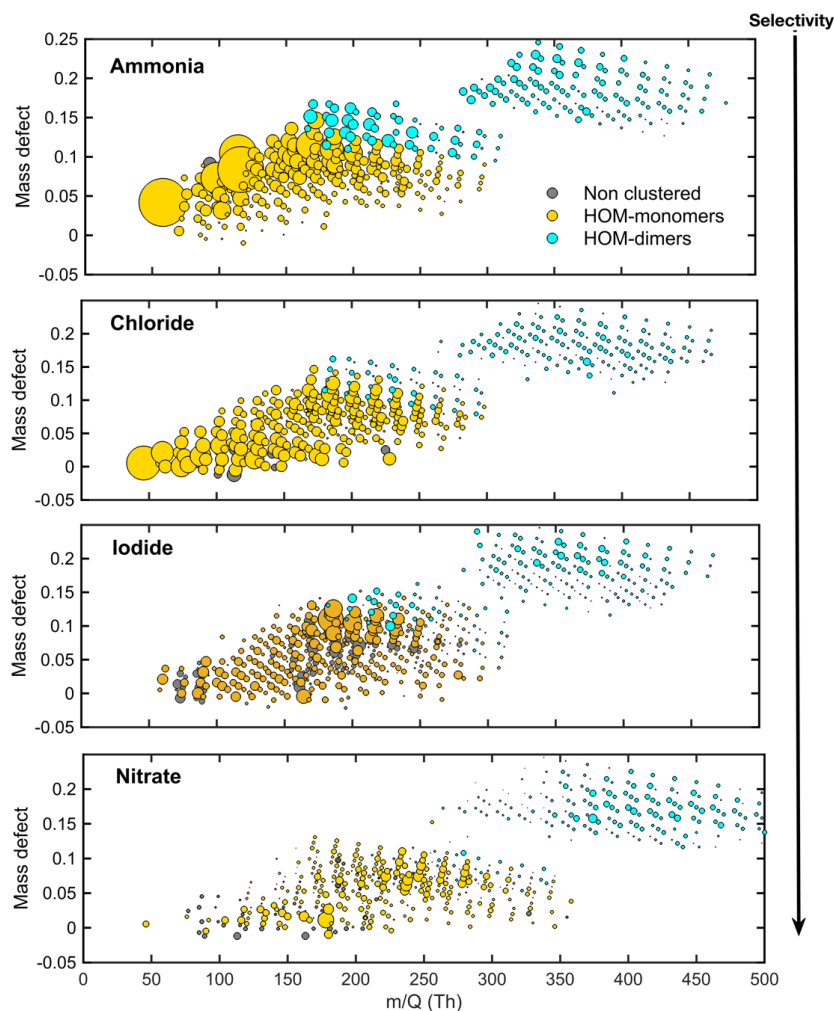
709 **Figure 3.** Impact of the relative humidity on the sensitivity of nitric acid, formic acid, and acrylic acid as a
710 function of different dopant concentrations (dopants: acetone, methanol, and acetonitrile). The x-axis
711 displays the partial pressure of water, corresponding to higher humidity levels within the reactor (0-100%
712 humidity). The color gradient indicates the increasing flow of specific dopants.
713



725 **Figure 4.** (A) presents the sensitivity dependence on the IMR pressure. The solid line represents the average
 726 sensitivity from six distinct Vocus AIM instruments, each normalized to one million reagent ions.
 727 Individual sensitivity measurements for each reactor are depicted as unique symbols. The error bars provide
 728 an estimate of the pressure gauge measurement uncertainty within 5 % of error. (B) shows the evolution of
 729 the sum of the reagent ions for Benzene cation chemistry and lower panel the ion signal intensity of toluene
 730 with and without normalization to reagent ions under a wide range of concentrations.

730

731



732

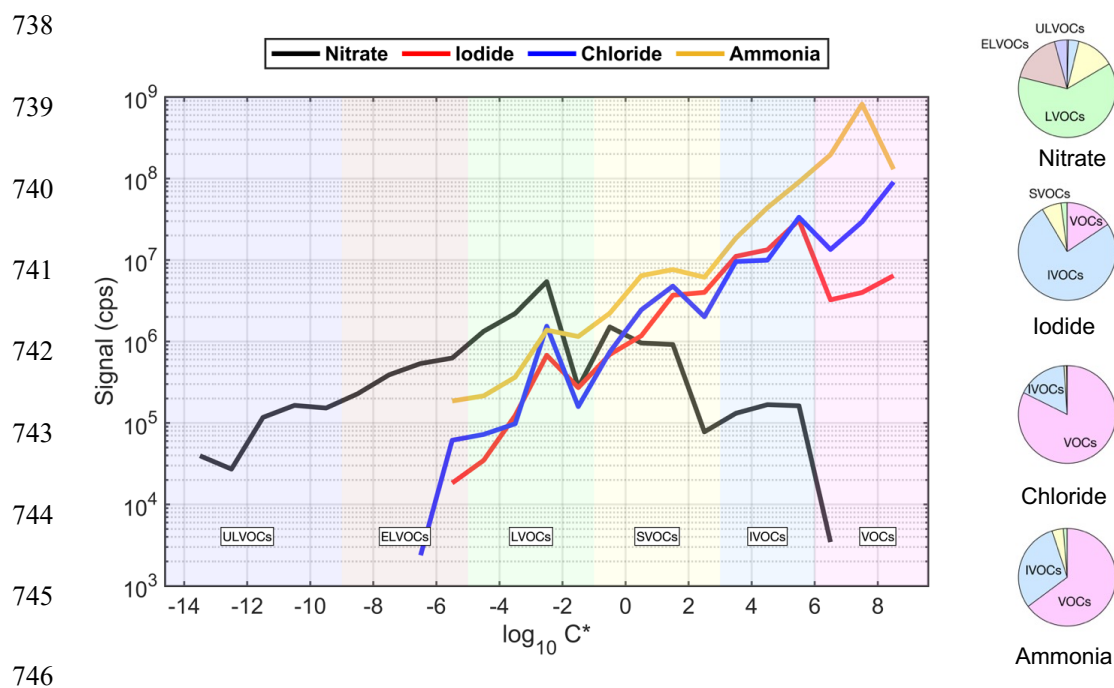
733 **Figure 5.** Mass defect plots of organic compounds measured by the Vocus AIM reactor using Ammonia,

734 Chloride, Iodide, and Nitrate ion chemistries generated via the O₃/OH initiated oxidation of α -pinene. The

735 x-axis represents the mass-to-charge ratio of the neutral analyte, and the y-axis represents the corresponding

736 mass defect, which is the difference between their exact mass and nominal mass.

737



747 **Figure 6.** Volatility distribution comparison for organic compounds detected by the Vocus AIM using
 748 nitrate, iodide, chloride, and ammonia ion chemistries. The background colors represent the saturation
 749 concentration (C_{sat}) in the range of ultra-low volatility (ULVOCs), extremely low volatility (ELVOCs), low
 750 volatility (LVOCs), semi-volatile (SVOCs), intermediate volatility (IVOCs), and volatile organic
 751 compounds (VOCs, pink). The pie charts represent the corresponding contributions of VOC, IVOC, SVOC,
 752 LVOC, ELVOC, and ULVOC classes from the O_3/OH initiated oxidation of α -pinene.

753